

# Hydrodynamic evolution of plasma waveguides for soft-x-ray amplifiers

Eduardo Oliva,<sup>1,2,\*</sup> Adrien Depresseux,<sup>3</sup> Manuel Cotelo,<sup>1,2</sup> Agustín Lifschitz,<sup>3</sup> Fabien Tissandier,<sup>3</sup> Julien Gautier,<sup>3</sup> Gilles Maynard,<sup>4</sup> Pedro Velarde,<sup>1,2</sup> and Stéphane Sebban<sup>3</sup>

<sup>1</sup>*Departamento de Ingeniería Energética, E.T.S.I. Industriales, Universidad Politécnica de Madrid, Madrid 28006, Spain*

<sup>2</sup>*Instituto de Fusión Nuclear, Universidad Politécnica de Madrid, Madrid 28006, Spain*

<sup>3</sup>*Laboratoire d'Optique Appliquée, ENSTA ParisTech, École Polytechnique ParisTech, CNRS, UMR7639, 91761, Palaiseau, France*

<sup>4</sup>*Laboratoire de Physique des Gaz et des Plasmas, CNRS, Université Paris-Sud bat. 210, 91405 Orsay, France*



(Received 8 November 2017; published 13 February 2018)

High-density, collisionally pumped plasma-based soft-x-ray lasers have recently delivered hundreds of femtosecond pulses, breaking the longstanding barrier of one picosecond. To pump these amplifiers an intense infrared pulse must propagate focused throughout all the length of the amplifier, which spans several Rayleigh lengths. However, strong nonlinear effects hinder the propagation of the laser beam. The use of a plasma waveguide allows us to overcome these drawbacks provided the hydrodynamic processes that dominate the creation and posterior evolution of the waveguide are controlled and optimized. In this paper we present experimental measurements of the radial density profile and transmittance of such waveguide, and we compare them with numerical calculations using hydrodynamic and particle-in-cell codes. Controlling the properties (electron density value and radial gradient) of the waveguide with the help of numerical codes promises the delivery of ultrashort (tens of femtoseconds), coherent soft-x-ray pulses.

DOI: [10.1103/PhysRevE.97.023203](https://doi.org/10.1103/PhysRevE.97.023203)

## I. INTRODUCTION

The performance of laser-driven plasma sources, whether for production and amplification of radiation (soft-x-rays) or particle acceleration, is usually limited by the length of laser-plasma interaction. Processes like diffraction and refraction defocusing disperse the infrared (IR) beam, shortening the interaction region. These deleterious effects are increasingly dominant at higher plasma density. Thus, some kind of waveguide is necessary to overcome this bottleneck.

There are several waveguiding techniques that allow intense ( $I > 10^{18} \text{ W cm}^{-2}$ ) IR pulses to propagate over several Rayleigh lengths in dense plasmas. At low densities ( $n_e \approx 10^{18} \text{ cm}^{-3}$ ) capillary discharge waveguides have been extensively studied and demonstrated [1–3]. In these devices the total reflection of the guided beam at the inner walls of a dielectric capillary tube allows the guiding of the laser beam. At higher electron densities relativistic self-focusing [4] can be a viable focusing mechanism since it is possible to attain its threshold power [5]  $P_{\text{th}} \approx 1.7 \times 10^{10} \frac{n_c}{n_e} \text{ W}$ , where  $n_c$  is the plasma critical density and  $n_e$  the electron density. To have a successful guiding over long distances it is required to maintain the pulse power over the threshold during all the propagation length. This is difficult due to competing effects like diffraction, over-ionization-induced refraction, instabilities, etc. Another method consists in creating a preformed plasma channel that will act as a waveguide [6]. The use of plasma waveguides at high densities ( $n_e > 10^{19} \text{ cm}^{-3}$ ), where the IR pulse propagates over several millimeters or even centimeters, has been demonstrated recently to create a  $\text{Kr}^{8+}$

plasma amplifier [7–9]. The plasma waveguide is created with the ignitor-heater technique using an axicon lens [8,10]. In this paper we will describe the creation and diagnosis of a plasma waveguide capable of guiding ultraintense IR pulses ( $I \approx 3 \times 10^{18} \text{ W cm}^{-2}$ ) over a length that varies from 5 mm to 3 cm. The layout of the paper is as follows. In Sec. II we will describe the experiment (Sec. II A) and the characterization of the plasma waveguide: its temporal evolution and guiding efficiency (Sec. II B). Section III will be dedicated to present the modeling of the experiment using hydrodynamic (Sec. III A) and particle-in-cell codes (Sec. III B). Finally, the results of this paper along with future lines of research will be summarized in Sec. IV.

## II. CREATION AND DIAGNOSIS OF AN OPTICALLY PREFORMED PLASMA WAVEGUIDE

A plasma can act as a waveguide provided the radial electron density is properly engineered. The refractive index of a plasma is given by  $\eta = \sqrt{1 - \frac{n_e(r)}{n_c}}$ , where  $n_e(r)$  is the radial density profile,  $n_c = \frac{m_e \epsilon_0 \omega^2}{e^2}$  is the critical density of the plasma,  $m_e$  is the electron's mass,  $\epsilon_0$  the vacuum permittivity,  $\omega$  the angular frequency of the electromagnetic field, and  $e$  the electron's charge. One can see that a lower electron density on axis will create appropriate conditions for guiding since the induced refraction overcomes the defocusing effects, allowing an intense IR laser to propagate through a high-density plasma over several Rayleigh lengths. Because of this radial profile, the waveguide is also referred as a plasma channel.

The creation of the plasma waveguide is a hydrodynamic process relying on the radial expansion of a previously created, elongated plasma [6]. To preform a plasma waveguide over all

\*eduardo.oliva@upm.es

the required length an axicon lens [11] has been used. This optical component longitudinally focuses a beam over a long distance. The angular aperture of its conical shape determines the length over which an incoming beam can be tightly focused uniformly.

In the research reported on this paper a double pulse scheme, known as the ignitor-heater technique, has been used [7,12]. This scheme is based on the decoupling of ionization and plasma heating processes. A first, ultrashort (a few tens of femtoseconds) pulse, named ignitor, generates the first electrons, creating the plasma. The second, long (hundreds of picoseconds) pulse, the heater, heats the free electrons of the plasma mainly via inverse Bremsstrahlung [13]. This increase in electron temperature triggers ongoing collisional ionization that takes place during and after the duration of the heater pulse (several nanoseconds). After this increase of electron density, the hydrodynamic evolution of the plasma leads to the formation of the waveguide. Hot electrons quickly diffuse out of the axis. Due to the significant difference in mass between electrons and ions, the motion of the latter will be slower. The resulting space charge region will induce an electric field that will slow down electrons and speed up ions. As a result, both ions and electrons expand radially at the speed of sound,

$$c_s = \sqrt{\bar{Z} \frac{k_B T_e}{m_i}}, \quad (1)$$

where  $c_s$  is the sound velocity,  $\bar{Z}$  the mean ionization,  $T_e$  the electron temperature, and  $k_B$  Boltzmann's constant. This speed is of the order of tens of microns per nanosecond within the expected experimental parameters, a mean ionization value of  $3 \leq \bar{Z} \leq 6$  and an electron temperature  $T_e < 100$  eV. Thus, this plasma expansion creates a plasma waveguide with a radius of several tens of micrometers in few nanoseconds. When the density profile is steep enough to overcome diffraction the intense IR pulse is guided along the plasma. For example, when the electron density has a parabolic radial profile  $n_e(r) = n_{e1}[1 + (r/r_{e1})^2]$ , where  $n_{e1} = n_e(0)$  is the electron density at the center of the guide and  $r_{e1}$  is the radial coordinate where  $n_e(r_{e1}) = 2n_{e1}$ , guiding is achieved when  $Z_R = r_{e1} \sqrt{\frac{n_c}{n_{e1}}}$ .  $Z_R$  is the Rayleigh length of the guided beam.

### A. Formation and evolution of the plasma waveguide

Experimentally, the waveguide is created by focusing two IR ( $\lambda = 800$  nm) pulses, the ignitor (130 mJ, 30 fs) and the heater (690 mJ, 600 ps) using an axicon lens, as shown in Fig. 1. The delay between the ignitor and heater pulse is fixed at 600 ps. The pulses are focused at a height  $h = 1.5$  mm of a  $5 \text{ mm} \times 500 \mu\text{m}$  nozzle with a backing pressure of 150 bar. These conditions correspond to a neutral krypton density of about  $n_0 = 10^{19} \text{ cm}^{-3}$ . The formation and subsequent hydrodynamic evolution of the plasma waveguide is observed using a frequency doubled probe beam. A Mach-Zehnder interferometer and an imaging system with large magnification (about 13) are used to measure the electron density profile of the plasma waveguide.

Figure 2 depicts the electron density at the center of the gas jet measured for different delays of the doubled frequency probe beam. The process is triggered when the ignitor pulse

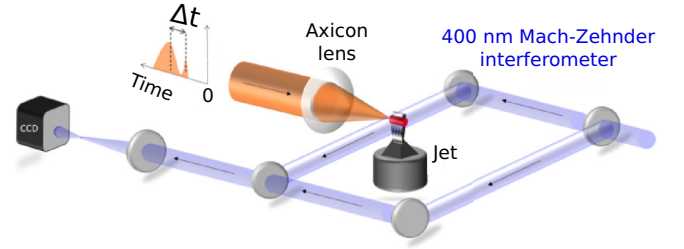


FIG. 1. Experimental setup for the creation and diagnosis of a high-density plasma waveguide. The ignitor and heater beams have, respectively, an energy of  $E_1 = 130$  mJ and  $E_2 = 690$  mJ, a duration of 30 fs and 600 ps and are separated by a delay of  $\Delta t = 600$  ps.

creates the first free electrons at the axis (Fig. 2, curve at  $t = 0$  ns). Posterior heating by the heater pulse and subsequent collisional ionization lead to an abrupt increase of the electron density (Fig. 2, during the first nanosecond). The formation of the plasma waveguide, due to hydrodynamic expansion, starts approximately one nanosecond after the arrival of the ignitor pulse and lasts for several nanoseconds, as depicted in Fig. 2, from  $t = 1$  ns till the end. The expansion speed can be measured, giving a value of  $v \approx 13 \mu\text{m/ns}$ . From Eq. (1) it is possible to infer a range for the electron temperature of  $T_e \approx 49$  eV if we assume that  $\bar{Z} = 3$  and  $T_e \approx 24.5$  eV when  $\bar{Z} = 6$  is assumed. The expansion velocity is a key parameter to optimize the seeding time of the IR pulse. The optimal coupling between beam and waveguide depends on the diameter of the waveguide and its radial density gradient and both parameters vary in time. Thus, modeling of the expansion velocity of the waveguide, presented in Sec. III, is needed to develop optimized high-density plasma waveguides.

### B. Guiding efficiency

Once the plasma waveguide is created and has evolved till the optimum time to seed the intense IR pulse to be guided, its performance can be stated by measuring the guiding efficiency, i.e., the percentage of energy of the IR pump beam that is transmitted throughout the length of the waveguide. This IR

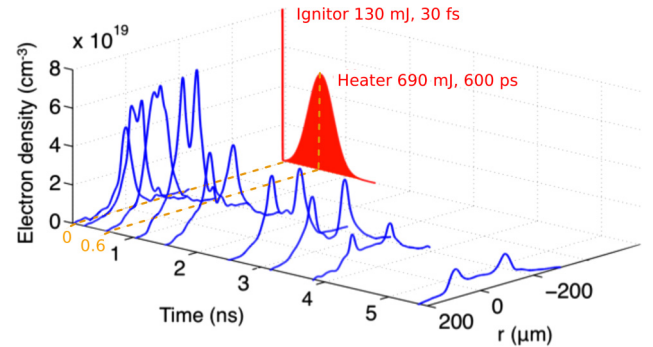


FIG. 2. Electron density at the central region of the 5-mm-long gas jet at different ignitor-probe delays, showing the creation and evolution of the plasma waveguide. The ignitor and heater pulse delay and duration are shown in the figure (the time at which the peak of the pulse arrives is shown in orange). Their relative intensities are not scaled for the sake of clarity.

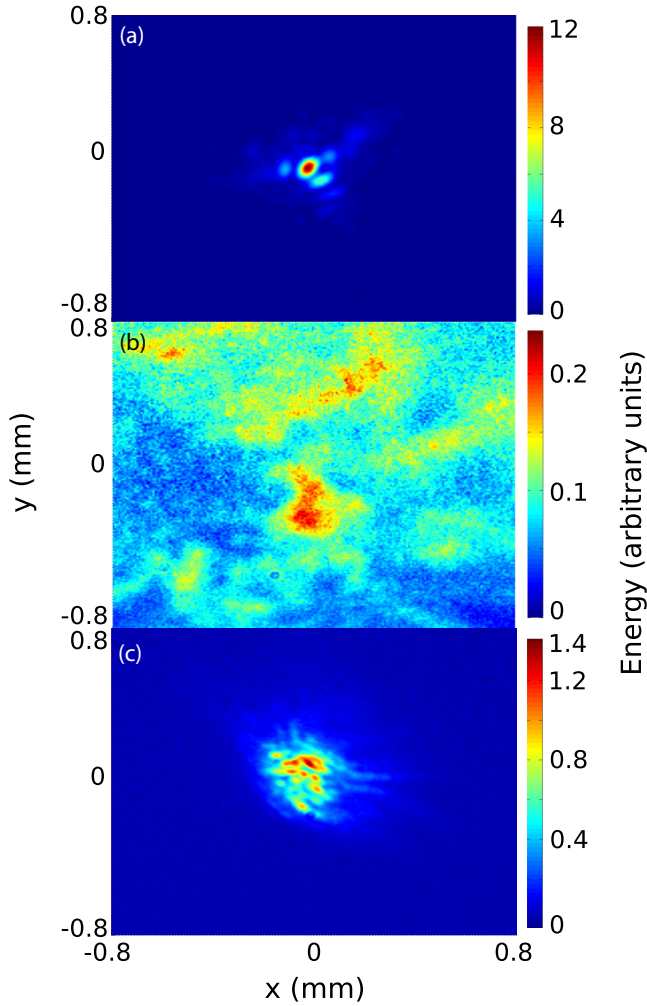


FIG. 3. Energy distribution of the IR pump beam ( $I = 3 \times 10^{18} \text{ W cm}^{-2}$ ), at its focal spot in vacuum (a) and focused at the end of the 5-mm-long high-density plasma amplifier without (b) and with (c) the plasma waveguide, injected 1.55 ns after the arrival of the ignitor pulse.

pulse ( $\lambda = 800 \text{ nm}$ ) has an energy of 1.36 J and a duration of 30 fs focused to a focal spot of  $38 \mu\text{m}$  in  $1/e^2$ -diameter. In these conditions, the intensity on target is about  $I = 3 \times 10^{18} \text{ W cm}^{-2}$  and the Rayleigh length is  $Z_R = 0.0725 \text{ cm}$ . This pulse is injected into the waveguide 1.55 ns after the arrival of the ignitor pulse, when the waveguide has a diameter of  $d \approx 80 \mu\text{m}$ . It is worth mentioning that the plasma waveguide diameter must be at least  $d = 2w_0$  where  $w_0$  is the beam waist. For lower diameters the coupling between the beam and the waveguide is not good, inducing strong losses at the entrance of the waveguide. For wider waveguides the transmitted energy does not improve. The reason is that the better coupling efficiency for wider waveguides is compensated by the lower radial density gradient, which reduces the guiding effect. Therefore, further plasma expansion does not significantly improve the overall waveguiding efficiency.

Figure 3(a) shows the energy distribution of the IR beam focused in vacuum. When this beam propagates through a 5-mm-long high-density plasma (without waveguide) it is strongly refracted and the signal measured at the output is very

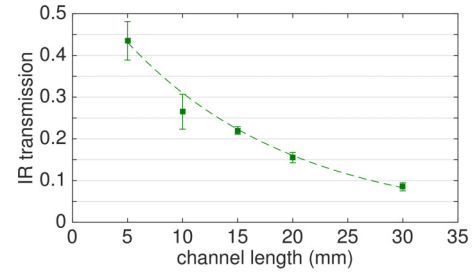


FIG. 4. Transmission of the IR beam through the plasma waveguide as a function of the gas jet length (which is similar to that of the plasma waveguide). The dashed green line denotes the best fit.

weak and divergent, as shown in Fig. 3(b). The main defocusing mechanism is over-ionization-induced refraction, allowing only less than 1% of the beam energy to be transmitted. When the IR beam propagates throughout a 5-mm-long high-density plasma waveguide it remains more or less collimated after seven Rayleigh lengths, as shown in Fig. 3(c). About 45% of the beam energy is transmitted. Leakage mainly comes from the coupling of the beam into the waveguide as well as the initial strong refraction imparted by the strong ionization at focus [14].

The plasma waveguide can be scaled in length. Figure 4 shows the transmitted energy of the IR pump beam at the end of 5 mm, 10 mm, 15 mm, 20 mm, and 30 mm plasma waveguides (or conversely, 7 Rayleigh lengths, 14 Rayleigh lengths, 20 Rayleigh lengths, 27 Rayleigh lengths, and 41 Rayleigh lengths) with electron density of  $n_e = 1.2 \times 10^{20} \text{ cm}^{-3}$ ,  $n_e = 9 \times 10^{19} \text{ cm}^{-3}$ ,  $n_e = 5.5 \times 10^{19} \text{ cm}^{-3}$ ,  $n_e = 3.4 \times 10^{19} \text{ cm}^{-3}$ , and  $n_e = 2.6 \times 10^{19} \text{ cm}^{-3}$ . It can be seen that the transmission decreases almost linearly with the waveguide length.

The diagnostic method used allows to ascertain the transmission of the plasma waveguide. However, several parameters of interest like the mean ionization of the plasma after the passage of the IR pump beam and the mechanism that dominates the leakage of energy at different plasma lengths cannot be deduced from the experimental results presented in this paper. For this reason, the propagation of the IR pump beam through the plasma waveguide is modeled with particle-in-cell codes. The results of the modeling, along with its shortcomings, are presented in Sec. III.

### III. COMPUTATIONAL RESULTS

In this section we will present the computational modeling of the experiment described in Sec. II. The two principal results aforementioned, the temporal evolution of the plasma waveguide and the transmittance of the IR pump beam, are studied, respectively, with a hydrocode and particle-in-cell codes.

The hydrodynamic expansion that creates the plasma waveguide is studied with the simulation code ARWEN [15]. ARWEN is a 2D radiative hydrodynamics code with adaptive mesh refinement (AMR) [16]. Compressible hydrodynamics are solved with an unsplit second-order Godunov method that allows for multimaterial hydrodynamics in both cartesian and cylindrical coordinates. Electron heat conduction is modeled with flux-limited diffusion solvers while radiation transport



is modeled using the discrete-ordinate method with synthetic acceleration [17] and multigroup capabilities adapted to AMR scheme [18,19]. The laser energy is deposited using a 3D raytracing method. This code has already been applied to different fields such as fast ignition [20], plasma-based soft-x-ray lasers [21–23] and laboratory astrophysics [24].

The propagation of an intense IR beam throughout the waveguide has been modeled with the 3D particle in cell (PIC) code CalderCirc [25]. This code solves the Maxwell and Vlasov equations in cylindrical coordinates. A number of Fourier components of the electric field are solved, depending on the degree of asymmetry of the problem. The presence of the plasma induces the coupling of the models, otherwise uncoupled being Maxwell equations linear. Thus, a simulation using  $m$  modes is roughly equivalent in computational terms to  $m$  bidimensional calculations. The macroparticles describing the plasma are advanced by solving the relativistic equations of motion  $\dot{\mathbf{P}} = q(\mathbf{E} + \frac{1}{c}\mathbf{v} \times \mathbf{B})$  and  $\dot{\mathbf{x}} = \frac{1}{m\gamma}\mathbf{P}$ , where  $\mathbf{P}$  is the canonical momentum,  $q$  the electric charge,  $\mathbf{E}$  and  $\mathbf{B}$  the electric and magnetic fields,  $\mathbf{v}$  the particle's velocity,  $m$  the particle's mass, and  $\gamma$  the relativistic factor. We also used the PIC code WAKE-EP [3], an upgrade of the quasistatic two-dimensional axisymmetric code WAKE [26]. WAKE-EP is a 2D fully relativistic, nonlinear, particle code that involves the following approximations that reduce the computational cost of the simulations but that are only valid for under-dense plasmas,  $\frac{\omega_p}{\omega_l} \ll 1$ , where  $\omega_p$  and  $\omega_l$  are, respectively, the plasma and laser frequencies. The interaction of the electrons with the electric field is separated in two components, the jitter due to the high-frequency laser field and the low-frequency response to the ponderomotive potential of the laser field envelope. A second approximation, the so-called quasistatic approximation (QSA), is also implemented, assuming that the characteristic time of deformation of the laser pulse envelope is longer than the electron transit time through the laser pulse. This code allows us to study long plasmas (of the order of centimeters or longer) and the gain on computational time allows us to perform a huge number of simulations with table top computers. For these reasons, plasma waveguides with lower density ( $n_e \sim 10^{18} \text{ cm}^{-3}$ ) were first modeled using WAKE-EP. The results of these simulations are useful to understand the different mechanisms that take place during the propagation of the IR beam [14]. To ascertain the validity of these low-density simulations to our problem, more expensive (in terms of computation time and memory) but also more accurate simulations were performed using CalderCirc.

### A. Hydrodynamics

The 3D formation and evolution of a 5-mm-long plasma waveguide has been modeled taking advantage of its cylindrical symmetry along the propagation axis. A 3D raytracing method is used to emulate the axicon lens and deposit the energy of the ignitor (130 mJ, 30 fs,  $\lambda = 800 \text{ nm}$ ) and heater (690 mJ, 600 ps,  $\lambda = 800 \text{ nm}$ ) beams in the  $5 \text{ mm} \times 500 \mu\text{m}$  krypton gas jet at a density of  $\rho = 1.39 \text{ kg/m}^3$ , corresponding to a neutral density of  $n_0 = 10^{19} \text{ cm}^{-3}$ . The laser deposition model only takes into account resonant absorption and inverse Bremsstrahlung and posterior thermalization via electron heat diffusion. While it is enough to model the absorption of long

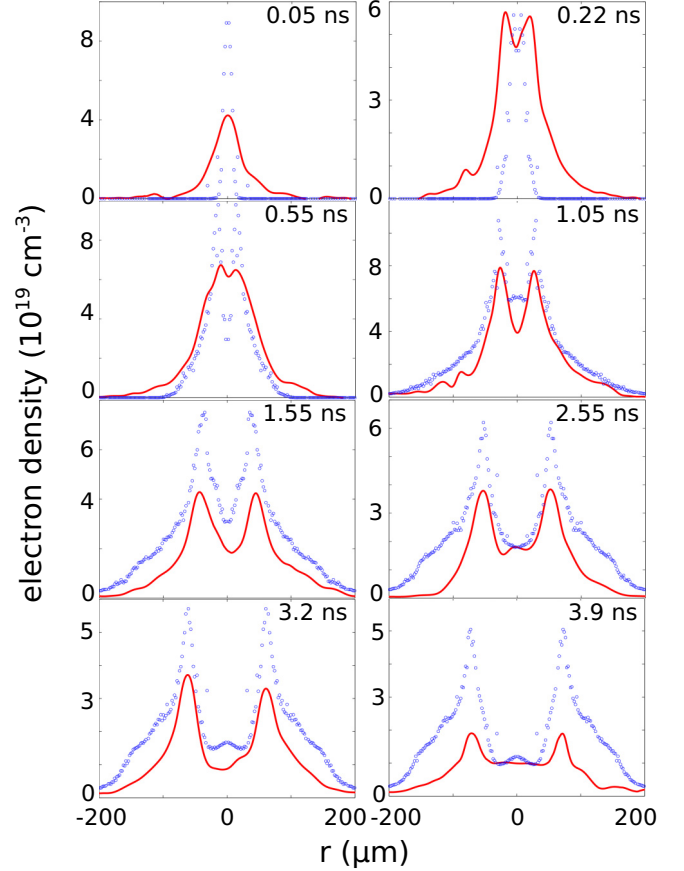


FIG. 5. Radial profile of electron density as measured experimentally (red continuous line) and as given by our modeling (blue circles) at different ignitor-probe delays.

(hundreds of picoseconds) laser pulses like the heater beam, the interaction with ultrashort pulses (tens of femtoseconds) requires to tweak the model when the ignitor pulse acts assuming that the plasma is doubly ionized when computing the absorption coefficient. Since the heater pulse arrives with a 600 ps delay and the waveguide starts to evolve 1 ns after the ignitor pulse arrives this tweak does not have an impact neither in the absorption of the heater pulse energy nor in the posterior evolution of the waveguide.

Figure 5 shows the radial profile of electron density in the plasma waveguide as measured experimentally (red continuous line) and as given by our hydrodynamics code (blue circles). It is clearly shown that, even with the tweak described above, our model starts reproducing experimental results only after 500 ps have passed since the arrival of the ignitor pulse. From this moment, the energy of the heater pulse is absorbed via inverse Bremsstrahlung while hydrodynamic expansion is the main mechanism that drives the plasma waveguide evolution. Both mechanisms, inverse Bremsstrahlung and hydrodynamic expansion, are well modeled by our code. The expansion velocity varies between 6.5 and  $10 \mu\text{m/ns}$  and the electron temperature at the center of the waveguide varies from a value of 45 eV at  $\Delta t = 1 \text{ ns}$  after the ignitor beam arrives and 12 eV at  $\Delta t = 3.9 \text{ ns}$ , in good agreement with the experimental results when the uncertainty on the mean ionization is taken into account.

While the expansion velocity and the general radial profile of the plasma waveguide are well modeled by our code, the electron density is overestimated by a factor of almost two. This is due to the fact that our code uses local thermodynamic equilibrium (LTE) tables to compute the ionization. The average ionization given by the code varies among  $\bar{Z} = 6$  and  $\bar{Z} = 12$ . Dividing by two these values gives a better adjustment of the radial electron density profile and an average ionization of  $3 \leq \bar{Z} \leq 6$ . Moreover, the electron density and temperature computed from the experimentally measured expansion velocity agrees with the model when the mean ionization is assumed to lie in the aforementioned range. Finally, as it will be shown in the next section, assuming the mean ionization to lie within this range ( $3 \leq \bar{Z} \leq 6$ ) allows PIC codes to reproduce the propagation and guiding of the intense IR pump pulse. Since it is well known that LTE ionization overestimates the average ionization compared to non-LTE solvers, a full computation of the transient ionization process is needed to improve the agreement between model and experiment and feed better data to particle-in-cell codes.

### B. Guiding efficiency

The 3D propagation of a 1.36 J, 30 fs ( $I = 3 \times 10^{18}$  W cm $^{-2}$ ) IR pump beam through a 5-mm plasma waveguide corresponding to experimental conditions has been studied with particle-in-cell codes to obtain the energy transmitted through the waveguide and to compare it with experimental results. In addition to this, density maps, given by CalderCirc, of the ion species present in the waveguide after the passage of the IR pump beam are also pictured. These maps allow us not only to unveil defocusing mechanisms like over-ionization-induced refraction but also to ensure that the transmitted IR pump beam has enough energy to produce the Kr $^{8+}$  ion, the lasing ion of a Ni-like krypton amplifier, all along the waveguide.

The experimentally measured radial density profile of the waveguide is approximated by using a Padé approximant with the following parameters:

$$\frac{n_e}{n_{e0}} = \frac{1 + r^2(a + br^2)}{1 + cr^6},$$

with  $n_{e0}$  the electron density in the axis of the waveguide ( $n_{e0} = 1.84 \times 10^{19}$  cm $^{-3}$  for experimental conditions),  $a = -2.2949 \times 10^{-4}$   $\mu\text{m}^{-2}$ ,  $b = 1.73762 \times 10^{-6}$   $\mu\text{m}^{-4}$ , and  $c = 2.88648 \times 10^{-10}$   $\mu\text{m}^{-6}$ . The density of ions is derived assuming a constant ionization stage close to the optical axis of the plasma waveguide. We consider a transverse profile of the mean ionization  $\bar{Z}$  given by

$$\frac{\bar{Z}}{\bar{Z}_0} = \frac{1 + \alpha r^2}{1 + \alpha r^2 + \beta r^6},$$

with  $\bar{Z}_0$  the average ionization in the axis of the waveguide,  $\alpha = 3 \times 10^{-8}$   $\mu\text{m}^{-2}$  and  $\beta = 1.2 \times 10^{-11}$   $\mu\text{m}^{-6}$ .

Figure 6 shows density maps of some krypton ion species, from Kr $^{5+}$  to Kr $^{10+}$ , created by the IR pump beam as given by CalderCirc. The presence of highly charged species all along the waveguide is a signature of guiding an intense enough pulse. The abundance of Kr $^{8+}$  in the last 3 mm of the plasma ensures its use as a soft-x-ray amplifier. In addition

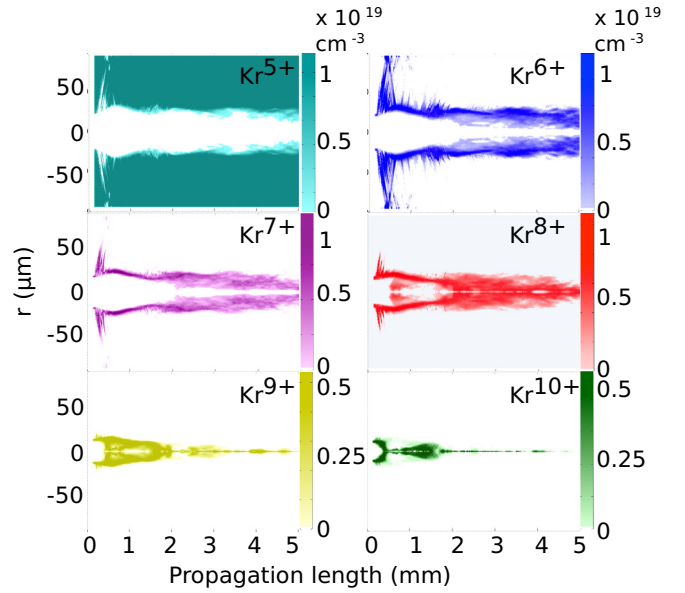


FIG. 6. Density maps of krypton ion species, as given by CalderCirc, generated focusing a IR beam with  $I = 3 \times 10^{18}$  W cm $^{-2}$  into a high-density 5-mm-long plasma waveguide, which corresponds to experimental conditions. Each subfigure shows the density of the corresponding ion species.

to this, the presence of highly charged species (Kr $^{10+}$  and higher, not depicted here) during the first millimeter hints that most of the leaks take place at the entrance of the plasma waveguide, due to strong refraction induced by this over-ionization. When the initial ionization is supposed to be  $\bar{Z}_0 = 5$  (well within the bounds given by our hydrodynamic simulations) the transmission of the waveguide computed by the code agrees with the experimental value. However, the transmission strongly depends on the initial average ionization. The lower the average ionization, the lower the transmission is. Indeed, if the initial ionization is taken to be  $\bar{Z}_0 = 3$  the transmission of the waveguide drops to 10%. This effect can be a numerical artifact caused by the fact that the pump beam duration may become longer than the simulation moving window, thus artificially lowering the value of the total energy at the output of the waveguide. However, further simulations and experiments are needed to ascertain precisely the role of the average ionization of the plasma.

Simulations at lower densities can give useful insights about the mechanisms involved in guiding while being less computationally demanding, thus complementing the previous one. It is worth mentioning that lower-density plasma waveguides are still of interest for plasma based soft-x-ray lasers and laser-plasma electron acceleration. For this reason, we have conducted simulations with the 2D axisymmetric PIC code WAKE-EP at lower densities. Figure 7 shows the fraction of energy guided (blue circles) and unguided (magenta squares) through the plasma waveguide for different electron densities at its axis. These fractions are computed as follows: at a given instant, the fraction of energy guided is considered to be the ratio of the energy contained within the limits of the plasma waveguide over the total initial energy. Conversely, the fraction of unguided energy is computed as the ratio of

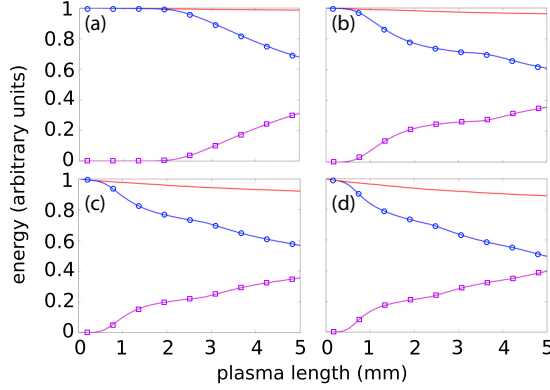


FIG. 7. Fraction of the energy of the IR beam propagating through the waveguide, as computed by WAKE-EP, guided (blue circles) and unguided (magenta squares) for different axial electron densities: (a)  $n_{e0} = 10^{18} \text{ cm}^{-3}$ , (b)  $n_{e0} = 3 \times 10^{18} \text{ cm}^{-3}$ , (c)  $n_{e0} = 5 \times 10^{18} \text{ cm}^{-3}$ , and (d)  $n_{e0} = 8 \times 10^{18} \text{ cm}^{-3}$ . The sum of both is depicted by the red continuous line.

the energy inside the simulation domain but outside the limits of the plasma waveguide over the total initial energy. The initial average ionization at the axis is assumed to be  $\bar{Z}_0 = 3$  and the density at the peaks of the channel is assumed to be twice than the one at the axis. The red curve is the sum of both curves, i.e., the total energy in the system. It decreases slowly due to losses through the absorbing boundaries of the simulation window. For axial densities of (a)  $n_{e0} = 10^{18} \text{ cm}^{-3}$ , (b)  $n_{e0} = 3 \times 10^{18} \text{ cm}^{-3}$ , (c)  $n_{e0} = 5 \times 10^{18} \text{ cm}^{-3}$ , and (d)  $n_{e0} = 8 \times 10^{18} \text{ cm}^{-3}$ , the respective transmittances are 68%, 61%, 57%, and 49%. This trend indicates that the transmittance at experimental conditions should be lower than measured experimentally, in agreement with the full PIC simulations when using an initial ionization of  $\bar{Z}_0 = 3$ . In conclusion, a higher mean ionization of the channel,  $\bar{Z}_0 = 5$ , allows the full 3D PIC simulations to explain the experimental IR pump beam transmittance and it is well within the bounds given by experimental results and hydrodynamic modeling. In addition to this, the inferred electron temperature for this mean ionization,  $T_e = 29.4 \text{ eV}$ , agrees with the electron temperature given by our hydrocode at  $t = 1.55 \text{ ns}$ , the injection time of the IR pump pulse.

Figure 7 also shows that a strong leakage takes place during the first millimeter of propagation. The higher the density, the stronger is this leakage and the earlier it happens. This is a clear signature of the over-ionization-induced refraction phenomenon at the entrance of the waveguide [14]. The intensity of the IR pump pulse is high enough to sustain highly charged species (as shown in Fig. 6) and, as a result, a strong electron density gradient that overcomes the focusing effect of the waveguide, reducing the intensity of the transmitted pulse. When the intensity is low enough so only  $\text{Kr}^{8+}$  is sustained in most of the channel ( $I \approx 10^{17} \text{ W cm}^{-2}$ ), the waveguide profile is retrieved and the IR pump pulse propagates. However, the initial distortion affects the coupling between beam and waveguide and a continuous leakage takes place. Since both the initial refraction and further leakage strongly depend on the initial state of the plasma (mean ionization, electron density),

further simulations coupled with hydrodynamic codes are needed.

#### IV. CONCLUSIONS

In this paper we have presented experimental results describing the formation and evolution of a plasma waveguide intended for the amplification of ultrashort pulses of soft-x-ray radiation. Radial electron density profiles at different stages of evolution were compared with a hydrodynamic model while the measured transmittance of the waveguide was studied with particle-in-cell codes. From  $t = 500 \text{ ps}$  since the arrival of the ignitor pulse, that creates the preplasma, the nanosecond evolution of the waveguide, i.e., its diameter and expansion velocity, is well modeled by the hydrodynamic code. This is a clear signature that the main processes that drive the evolution of the waveguide are hydrodynamic, while the heater pulse energy is mainly absorbed by inverse Bremsstrahlung. The radial expansion velocity is  $v \approx 10 \text{ } \mu\text{m/ns}$ . However, electron density and mean ionization are overestimated by a factor of two in our modeling. This is caused by the use of the local thermodynamic equilibrium approximation to compute the mean ionization. The experimental electron density profile is better fit when dividing computational results by two. Consequently, the mean ionization must lie in the range  $3 \leq \bar{Z} \leq 6$ . Particle-in-cell simulations modeling the propagation of intense IR pulses through the waveguide support this conclusion, since the measured transmission of the IR pump pulse is reproduced when  $\bar{Z} = 5$ . The electron temperature inferred from this ionization is  $T_e = 29.4 \text{ eV}$ , which agrees with the temperature given by our hydrodynamics simulations at the time the IR pump pulse is injected ( $t = 1.55 \text{ ns}$ ). In conclusion, experimental results combined with hydrodynamic and PIC simulations have allowed us to unveil the temporal evolution of the plasma waveguide electron density (shown in Fig. 2), its radial expansion velocity,  $v \approx 10 \text{ } \mu\text{m/ns}$ , mean ionization  $\bar{Z} = 5$ , and electron temperature  $T_e = 29.4 \text{ eV}$  when the IR pump pulse is injected at  $t = 1.55 \text{ ns}$ . Since carefully tailored high-density plasma waveguides are expected to deliver pulses shorter than  $100 \text{ fs}$  [9], further hydrodynamic and particle-in-cell modeling will ensure the optimization of this promising ultra-intense soft-x-ray source.

#### ACKNOWLEDGMENTS

The authors acknowledge useful discussions with A. González, P. Martínez, J. Moreno, and E. Vázquez. This work has been supported by the French National Research Agency Project No. ANR-11-BS04-0023 ROLEX and by “Investissements d’avenir” Labex PALM (Grant No. ANR-10-LABX-0039-PALM), by the Spanish Ministerio de Educación, Cultura y Deporte through the Plan Nacional research program, Grant No. ENE2012-32108, the EUROfusion Consortium (Grant No. AWP15-ENR-01/CEA-02), the People Programme (Marie Curie Actions) of the European Union’s Seventh Framework Programme (FP7/2007-2013) under REA Grant Agreement No. 627191, project DAGON, and the European Union’s Horizon 2020 research and innovation programme under Grant Agreement No. 665207 VOXEL.

- [1] C. Courtois, A. Couaïron, B. Cros, J. R. Marquès, and G. Matthieussent, *Phys. Plasmas* **8**, 3445 (2001).
- [2] W. P. Leemans, B. Nagler, A. J. Gonsalves, C. Tóth, K. Nakamura, C. G. R. Geddes, E. Esarey, C. B. Schroeder, and S. M. Hooker, *Nat. Phys.* **2**, 696 (2006).
- [3] B. S. Paradkar, B. Cros, P. Mora, and G. Maynard, *Phys. Plasmas* **20**, 083120 (2013).
- [4] C. E. Max, J. Arons, and A. B. Langdon, *Phys. Rev. Lett.* **33**, 209 (1974).
- [5] P. Sprangle, C.-M. Tang, and E. Esarey, *IEEE Trans. Plasma Sci.* **15**, 145 (1987).
- [6] C. G. Durfee and H. M. Milchberg, *Phys. Rev. Lett.* **71**, 2409 (1993).
- [7] M.-C. Chou, P.-H. Lin, C.-A. Lin, J.-Y. Lin, J. Wang, and S.-Y. Chen, *Phys. Rev. Lett.* **99**, 063904 (2007).
- [8] P.-H. Lin, M.-C. Chou, C.-A. Lin, H.-H. Chu, J.-Y. Lin, J. Wang, and S.-Y. Chen, *Phys. Rev. A* **76**, 053817 (2007).
- [9] A. Depresseux, E. Oliva, J. Gautier, F. Tissandier, J. Nejd, M. Kozlova, G. Maynard, J.-P. Goddet, A. Tafzi, A. Lifschitz, H. T. Kim, S. Jacquemot, V. Malka, K. Ta Phuoc, C. Thauray, P. Rousseau, G. Iaquaniello, T. Lefrou, A. Flacco, B. Vodungbo, G. Lambert, A. Rousse, P. Zeitoun, and S. Sebban, *Nature Photon.* **9**, 817 (2015).
- [10] Y.-F. Xiao, H.-H. Chu, H.-E. Tsai, C.-H. Lee, J.-Y. Lin, J. Wang, and S.-Y. Chen, *Phys. Plasmas* **11**, L21 (2004).
- [11] J. H. McLeod, *J. Opt. Soc. Am.* **44**, 592 (1954).
- [12] A. Butler, A. J. Gonsalves, C. M. McKenna, D. J. Spence, S. M. Hooker, S. Sebban, T. Mocek, I. Bettiabi, and B. Cros, *Phys. Rev. A* **70**, 023821 (2004).
- [13] S. Eliezer, *The Interaction of High-Power Lasers with Plasmas* (Institute of Physics Publishing, Bristol, UK, 2002).
- [14] E. Oliva, A. Depresseux, F. Tissandier, J. Gautier, S. Sebban, and G. Maynard, *Phys. Rev. A* **92**, 023848 (2015).
- [15] F. Ogando and P. Velarde, *J. Quant. Spectrosc. Radiat. Transf.* **71**, 541 (2001).
- [16] M. J. Berger and J. Olier, *J. Comput. Phys.* **53**, 484 (1984).
- [17] M. L. Adams and E. W. Larsen, *Prog. Nucl. Energy* **40**, 3 (2002).
- [18] M. Gonzalez, C. García-Fernández, and P. Velarde, *Ann. Nucl. Energy* **36**, 886 (2009).
- [19] C. García-Fernández, P. Velarde, and M. Cotel, *IEEE Trans. Plasma Sci.* **38**, 2359 (2010).
- [20] P. Velarde, F. Ogando, S. Eliezer, J. Martínez-Val, J. Perlado, and M. Murakami, *Laser Part. Beams* **23**, 43 (2005).
- [21] K. Cassou, P. Zeitoun, P. Velarde, F. Roy, F. Ogando, M. Fajardo, G. Faivre, and D. Ros, *Phys. Rev. A* **74**, 045802 (2006).
- [22] E. Oliva, P. Zeitoun, S. Sebban, M. Fajardo, P. Velarde, K. Cassou, and D. Ros, *Opt. Lett.* **34**, 2640 (2009).
- [23] E. Oliva, P. Zeitoun, P. Velarde, M. Fajardo, K. Cassou, D. Ros, S. Sebban, D. Portillo, and S. le Pape, *Phys. Rev. E* **82**, 056408 (2010).
- [24] M. Cotel, P. Velarde, A. de la Varga, D. Portillo, C. Stehlé, U. Chaulagain, M. Kozlova, J. Larour, and F. Suzuki-Vidal, *High Energy Dens. Phys.* **17**, 68 (2015).
- [25] A. Lifschitz, X. Davoine, E. Lefebvre, J. Faure, C. Rechatin, and V. Malka, *J. Comput. Phys.* **228**, 1803 (2009).
- [26] P. Mora and T. M. Antonsen, Jr., *Phys. Plasmas* **4**, 217 (1997).